Time-Resolved Fluorescence Allows Selective Monitoring of Trp30 Environmental Changes in the Seven-Trp-Containing Human Pancreatic Lipase†

Paul Ramos,‡,§ Thierry Coste,|| Etienne Piémont,‡ Jean Marc Lessinger,§ Jean Alain Bousquet,‡ Catherine Chapus,|| Brigitte Kerfelec,|| Georges Férard,§ and Yves Mély*,‡

Laboratoire de Pharmacologie et Physico-Chimie des Interactions Cellulaires et Moléculaires, UMR 7034 CNRS, Faculté de Pharmacie, Université Louis Pasteur, Strasbourg 1, 74, Route du Rhin, 67401 ILLKIRCH Cedex, France, Laboratoire de Biochimie Appliquée, U392 INSERM, Faculté de Pharmacie, Université Louis Pasteur, Strasbourg 1, 74, Route du Rhin, 67401 ILLKIRCH Cedex, France, and Faculté de Médecine, U476 INSERM, 27 Bd Jean Moulin, 13385 Marseille Cedex 5, France

Received May 27, 2003; Revised Manuscript Received August 29, 2003

ABSTRACT: Human pancreatic lipase (HPL, triacylglycerol acylhydrolase, EC 3.1.1.3) is a carboxyl esterase which hydrolyzes insoluble emulsified triglycerides and is essential for the efficient digestion of dietary fats. Though the three-dimensional structure of this enzyme has been determined, monitoring the conformational changes that may accompany the binding of various substrates and inhibitors is still of interest. Because of its sensitivity and ease of use, fluorescence spectroscopy of the intrinsic Trp residues is ideally suited for this purpose. However, the presence of seven Trp residues spread all over the HPL structure renders the interpretation of the fluorescence changes difficult with respect to the identification and location of the conformational or environmental changes taking place at the various Trp residues. In this context, the aim of this work was to investigate the contribution of the individual Trp residues to the fluorescence properties of HPL. To this end, we analyzed the steady-state and time-resolved fluorescence parameters of five single-point mutants in which one Trp residue was substituted with a weakly fluorescent Phe residue. In addition to the Trp residues at positions 30, 86, and 252, strategically located with respect to the active site, we also mutated Trp residues at positions 17 and 402, as representative residues of the HPL N- and C-terminal domains, respectively. Taken together, our data suggested that the solvent-exposed Trp30 residue contributed to at least 44% of the overall fluorescence of wild-type HPL. Moreover, we found that the long-lived fluorescence lifetime (6.77 ns) of wild-type HPL could be specifically attributed to Trp30, a feature that enables selective monitoring of its environmental changes. Additionally, Trp residues at positions 17 and 402 strongly contributed to the 1.61 ns lifetime of HPL, while Trp residues at positions 86 and 252 contributed to the 0.29 ns lifetime.

Pancreatic lipase (triacylglycerol acylhydrolase, EC 3.1.1.3) plays a key role in dietary fat digestion in the intestine by converting insoluble long chain triglycerides into more polar products that are able to cross over the brush border membrane of enterocytes as mixed micelles with bile lipids. The water soluble enzyme hydrolyzes triglycerides at a water−lipid interface and differs from classic esterases in that its activity is dramatically increased upon binding to the lipid interface (*1*). In the duodenum, the accumulation of several natural surfactants on the oil droplets prevents lipase from binding to its substrate (*2*). This problem is circumvented by colipase, a small pancreatic protein that helps in the binding of productive lipase to the surfactant-coated oil droplets (*3*, *4*).

Our understanding of pancreatic lipase activation and catalysis has improved considerably thanks to the elucidation of the three-dimensional structures of the uncomplexed human lipase (*5*) and of a human lipase−porcine colipase complex obtained in the presence of mixed micelles (*6*). Pancreatic lipase is made up of a single polypeptide chain organized in two domains. The large N-terminal domain (residues 1−336) bears the active site with the Ser152-Asp176-His263 catalytic triad, while the C-terminal domain (residues 337−449) is mainly devoted to colipase binding. In the uncomplexed lipase, the active site is covered by a large amphiphilic loop (the flap), which may account for the very weak activity of lipase in solution. In the lipase−colipase complex, the active site is exposed to the solvent, because of the motion of the flap, which establishes additional contacts with colipase. These findings provided a comprehensive view of the conformational changes in lipase during activation. The motion of the flap, by unmasking the active site and creating the oxyanion hole, converts the enzyme from an inactive (closed flap) to a catalytically active (open flap) conformation. Moreover, the process generates a large hydrophobic surface which is likely to represent the interfacial binding site.

Hermoso *et al.* (*7*) postulated that lipase activation occurs in the aqueous phase through the formation of an activated

† This work was supported by the CNRS and Université Louis Pasteur.

* To whom correspondence should be addressed. Telephone: +33(0)390244263. Fax: +33(0)390244312. E-mail: mely@pharma.u-strasbg.fr.

‡ UMR 7034 CNRS, Faculté de Pharmacie, Université Louis Pasteur.

§ U392 INSERM, Faculté de Pharmacie, Université Louis Pasteur.

|| U476 INSERM Faculté de Médecine.

10.1021/bi034900e CCC: $25.00
Published on Web 10/07/2003

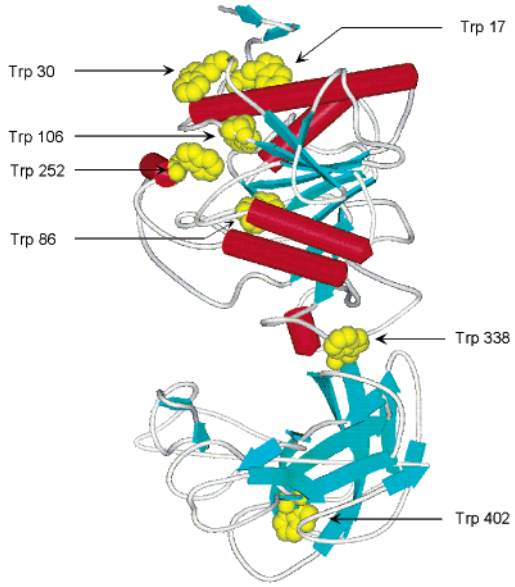

FIGURE 1: Three-dimensional structure of HPL (*19*). The calculated fractions of solvent exposure for the various Trp residues are as follows: Trp17 (0.07), Trp30 (0.23), Trp86 (0.02), Trp106 (0.0), Trp252 (0.05), Trp338 (0.09), and Trp402 (0.0). These values are in reasonable agreement with those previously calculated (*18*) from the three-dimensional HPL structure of Winkler *et al*. (*5*). The Trp residues are shown in yellow.

lipase−colipase−mixed micelle ternary complex. The micelle interacts extensively with the concave face of colipase and the distal tip of the lipase C-terminal domain (notably, residues 401−404). Colipase plays a central role in the complex, accounting for its complex functions in lipase activation, lipase anchoring at the lipid interface, and lipase catalysis (*8*). The ternary complex is likely to represent, *in vivo*, the functional entity that is able to hydrolyze triglycerides. Therefore, lipase catalysis is a very complex phenomenon involving protein−protein and protein−lipid interactions.

Fluorescence spectroscopy which is sensitive to changes in tryptophan microenvironments has been used to obtain information about the overall structural properties and conformational changes of several lipolytic enzymes, such as hormone-sensitive lipase (*9*), fungal lipases (*10*−*16*), and bacterial lipases (*13*, *17*). Fluorescence studies have also been used to monitor HPL[1] conformational changes induced by acylation with an inhibitor (*18*). HPL contains seven Trp residues, five of them being part of the N-terminal domain of the enzyme, at positions 17, 30, 86, 106, and 252 (Figure 1). Noticeably, Trp86 is located in the HPL active site near the Ser-Asp-His catalytic triad; Trp30 is located close to this active site, and Trp252 is part of the flap domain (*19*). The Trp residues at positions 338 and 402 are part of the C-terminal domain, and are probably not significantly affected by structural changes around the active site. Because of the large number of Trp residues spread all over the HPL structure, the fluorescence changes observed on binding of substrates or inhibitors were difficult to interpret, notably with respect to the location and identification of the conformational or environmental changes taking place at the various Trp residues.

In this context, there is a strong need to investigate the contribution of the individual Trp residues to the fluorescence properties of wild-type HPL (wtHPL). To this end, we analyzed the steady-state and time-resolved fluorescence parameters of five single-point mutants in which one Trp residue was substituted with a weakly fluorescent Phe residue. In addition to the Trp residues at positions 30, 86, and 252, strategically located with respect to the active site, we also mutated Trp residues at positions 17 and 402, as representative residues of the N- and C-terminal domains. Despite the presence of seven Trp residues per protein, we found that the fluorescence of wtHPL is dominated by the fluorescence of the Trp30 residue and that the long-lived fluorescence lifetime of wtHPL could be specifically attributed to this Trp residue, a feature that enables selective monitoring of its environmental changes.

MATERIALS AND METHODS

The BaculoGold starter package and baculovirus pVL1393 transfer vector were from PharMingen (San Diego, CA). The X-Press insect culture medium was purchased from Bioproduct. Fetal calf serum and antibiotics were from Dutscher and Life Technologies, Inc. (Copenhagen, Denmark).

Cloning and Expression of the Human Pancreatic Lipase. The DNA fragment encoding human lipase was amplified by PCR from a human adult normal pancreas Gene Pool cDNA using 5′-CGGAATCGCGGATCCATGCTGCCAC-TTTGG-3′ as the 5′ primer and 5′-CGGAATTCTTAACA-CGGTGTGAGGGTGAGCAG-3′ as the 3′ primer. PCR was carried out under standard conditions with 5 min at 95 °C as the first step and then 0.5 min at 95 °C, 1 min at 55 °C, and 1 min at 72 °C for 25 cycles. After analysis by electrophoresis on a 1% agarose gel, the PCR fragment was purified and sequenced using the dideoxy chain termination method (*20*). Cloning into the *Bam*HI and *Eco*RI sites of the pVL1393 transfer vector was accomplished. The recombinant plasmid, pVL1393Hulip, was purified using the QIAfilter Plasmid Midi Kit (Qiagen) and then used for cotransfection into Sf21 insect cells. Transfections were performed as described in the Baculovirus Expression Vector System Manual using the BaculoGold starter package (PharMingen). Recombinant baculovirus were produced and purified as previously described by Ayvazian *et al*. (*21*).

Site-Directed Mutagenesis. Mutations were introduced into the pVL1393HuPL plasmid using the Transformer Site Directed Mutagenesis Kit (Clontech). Briefly, two oligonucleotide primers were simultaneously annealed to one strand of the denatured double-stranded plasmid, one primer introducing the desired mutation and the other one mutating the unique *Nde*I restriction site of the recombinant plasmids. The mutagenic primers introducing the desired mutation into the human lipase cDNA are as follows: W17F, 5′-GACTC-CCCATTCTCCGGAATTACGG-3′; W30F, 5′-CCCCTC-CATATATTGCCTTTCTCTCC-3′; W86F, 5′-GGGAGAA-GAGAACTTCCTGGCC-3′; W252F, 5′-CGGAATCTT-CGAAGGGACTCG-3′; and W402F, 5′-GGTTAAATTTA-TTTTCTATAACAATGTCATCAAC-3′.

After selection by *Nde*I restriction analysis, the presence of the desired mutation was ascertained by sequencing using

[1] Abbreviations: HPL, human pancreatic lipase; wtHPL, wild-type human pancreatic lipase; TDCNa, sodium taurodeoxycholate; CD, circular dichroism; FRET, fluorescence resonance energy transfer; DAS, decay-associated spectra; MEM, maximum entropy method.

the dideoxy chain termination method (*20*). The subsequent plasmids were then purified using the QIAfilter Plasmid Midi Kit (Qiagen).

Expression of Human Lipase and Mutated Proteins in Sf21 Cells and Purification. Sf21 cells were grown to a density of 10^6 cells/mL at 27 °C in 220 mL of X-Press medium containing penicillin (50 units/mL) and streptomycin (50 μg/mL). The recombinant baculoviruses were added to the cells at a multiplicity of infection of ~2. Five to six days postinfection, the cultures of infected Sf21 cells were harvested and centrifuged to remove cells and debris. The supernatants were dialyzed overnight at 4 °C against 2 mM Tris-HCl buffer (pH 7.5) and then loaded onto a 5 mL heparin−Sepharose CL-6B column (Amersham Pharmacia Biotech, Orsay, France) previously equilibrated in 10 mM Tris-HCl buffer (pH 7.5) containing 5 mM NaCl and 1 mM benzamidine. Elution was performed using a linear NaCl concentration gradient (from 5 to 300 mM). The protein elution profiles were followed spectrophotometrically at 280 nm, and the presence of mutated lipases was investigated by activity measurements, SDS−PAGE, and Western blotting.

Activity Measurements. Lipase activities were potentiometrically determined at pH 7.5 and 25 °C using 0.11 M emulsified triacylbutyrylglycerol (tributyrin) in 1 mM Tris-HCl buffer containing 0.1 M NaCl and 5 mM $CaCl_2$ in the presence of 1 mM sodium taurodeoxycholate [TDCNa (Sigma, St. Louis, MO)] and a 5-fold molar excess of colipase. One unit of lipase activity corresponds to the release of 1.0 μmol of fatty acid per minute.

Gel Electrophoresis and Western Blotting. Electrophoresis on 10 to 12% polyacrylamide gels was carried out in the presence of SDS as described by Laemmli (*22*). Western blots were performed according to the method of Burnette (*23*). The membranes were incubated for 1 h at room temperature with specific polyclonal anti-lipase antibodies from rabbit, and immunodetection was carried out using alkaline phosphatase-labeled goat anti-rabbit IgG.

Circular Dichroism and Steady-State Fluorescence Spectroscopy. Circular dichroism (CD) spectra were recorded at 20 °C using a Jobin-Yvon CD VI nitrogen-flushed dichrograph and a cell path length of 0.1 cm. The protein concentration ranged between 1.3 and 1.7 μM. Calibration was done with (+)-camphorsulfonic acid ($\Delta\epsilon_{290.5} = 2.37$ M^{-1} cm^{-1} and $\Delta\epsilon_{192.5} = -4.95$ M^{-1} cm^{-1}).

Steady-state fluorescence measurements were performed at 20 °C on a SLM48000 spectrofluorimeter, with a 2 nm bandwidth for excitation and an 8 nm bandwidth for emission. The excitation wavelength was set at 295 nm to excite selectively the Trp residues. Spectra were corrected for the wavelength dependence of the emission monochromator and photomultiplier. Quantum yields were determined by taking L-Trp in water ($\phi = 0.14$) as a reference (*24*). Quenching by acrylamide was carried out by adding aliquots from stock solutions to the HPL derivatives. The fluorescence intensity changes corrected for the dilution were recorded at the maximum emission wavelength for the various derivatives.

Time-Resolved Fluorescence Measurements. The time-resolved fluorescence measurements were carried out with the single-photon counting time-correlated technique, using the stable picosecond excitation pulses provided by a pulse-picked frequency-tripled Ti-sapphire laser (Tsunami, Spectra Physics) pumped by a Millenia X laser (Spectra Physics). The temperature was maintained at 20 °C. The excitation pulses were at 295 nm, with a repetition rate of 4 MHz. The emission was collected through a polarizer set at the magic angle and a 4 nm band-pass monochromator (Jobin-Yvon H10) at the indicated wavelength. The single-photon events were detected with a microchannel plate Hamamatsu R3809U photomultiplier coupled to a Phillips 6954 pulse preamplifier and recorded on a multichannel analyzer (Ortec 7100) calibrated at 25.5 ps/channel. The instrumental response function was recorded with a polished aluminum reflector, and its full width at half-maximum was 40 ps. Time-resolved data analysis was performed using the maximum entropy method (MEM) and the Pulse5 software. For the analysis of the fluorescence decays, a distribution of 200 equally spaced lifetime values on a logarithmic scale between 0.01 and 20 ns was used. In all cases, the χ^2 values were close to 1.0, and the weighted residuals as well as the autocorrelation of the residuals were randomly distributed around zero, indicating an optimal fit. Decay-associated spectra were calculated from the steady-state fluorescence spectra [$F_{ss}(\lambda)$], and the time-resolved intensity parameters [$\alpha_i(\lambda)$ and $\tau_i(\lambda)$] deduced from the distribution of lifetimes by

$$F_i(\lambda) = F_{ss}(\lambda)\alpha_i(\lambda)\tau_i(\lambda)/[\sum\alpha_i(\lambda)\tau_i(\lambda)] \qquad (1)$$

where $F_i(\lambda)$ is the fluorescence associated with component i at wavelength λ.

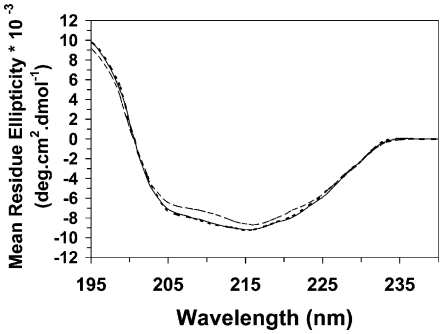

FIGURE 2: Far-UV CD spectra of wtHPL (—), F252HPL (− − −), and F30HPL (···) in phosphate buffer (pH 7.4) at 20 °C.

RESULTS

Structural and Functional Properties of the HPL Mutants. Purification of recombinant wtHPL and mutant human lipases was achieved as reported in Materials and Methods. To assess the contribution of individual Trp residues from the comparison of single-point mutants with wtHPL, one critical condition is that the folding of the mutants does not differ from that of the wtHPL. To address this point, the CD spectra of the various mutants were compared to the spectra of the native protein under the same conditions. The similarity of the CD spectra (Figure 2) strongly suggested that the mutation of the Trp residue at either position 17, 30, 86, 252, or 402 does not dramatically alter the secondary structure of HPL.

In a second step, the activity of the various proteins was determined on 0.11 M tributyrin in the presence of 1 mM TDCNa and a molar excess of colipase (Table 1). The F17HPL mutant was found to be as active as the wtHPL

Table 1: Specific Activity and Steady-State Fluorescence Parameters of wtHPL and Mutants[a]

	specific activity[b] (units/mg)	λ_{max} (nm)[b]	ϕ[b]	$\Delta\lambda_{1/2}$ (nm)[b]
wtHPL	8600 ± 50	336 ± 1	0.071 ± 0.002	61 ± 2
F17HPL	8900 ± 150	336 ± 1	0.097 ± 0.004	59 ± 1
F30HPL	6110 ± 180	327 ± 1	0.046 ± 0.002	50 ± 2
F86HPL	2160 ± 120	338 ± 1	0.105 ± 0.008	59 ± 1
F252HPL	5380 ± 80	340 ± 1	0.101 ± 0.003	59 ± 1
F402HPL	3200 ± 200	339 ± 1	0.089 ± 0.005	57 ± 1

[a] The specific activity of wtHPL and mutants was determined on 0.11 M tributyrin in the presence of 1 mM TDCNa and colipase. [b] Fluorescence experiments were performed in 20 mM Tris buffer (pH 7.5). The excitation wavelength was 295 nm. The maximum emission wavelength (λ_{max}), the quantum yield (ϕ), and the width at half-maximum of the emission spectrum ($\Delta\lambda_{1/2}$) are expressed as means ± the standard error of the mean for at least three experiments.

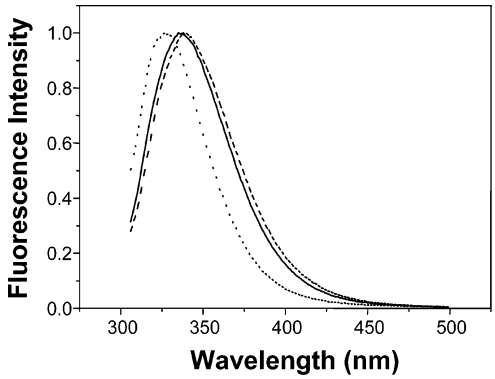

FIGURE 3: Emission spectra of HPL derivatives. The concentrations of wtHPL (—), F30HPL (•••), and F252HPL (– – –) were ~2 μM in 20 mM Tris buffer (pH 7.5). The excitation wavelength was set at 295 nm. The spectra were normalized at their maximum emission wavelength.

protein, suggesting that Trp17 does not interfere either directly or indirectly with catalysis. In contrast, the low activity of F86HPL and F402HPL could be related to the particular position of the mutations. W86, located in the entry of the active site pocket, might be part of the substrate recognition site, as suggested by Hermoso *et al*. (*25*). Therefore, the mutation of this residue may result in an incorrect orientation of the substrate in the active site that is unfavorable for efficient catalysis. Likewise, the mutation of W402 located close to the micelle and colipase binding sites might hamper the formation of a fully functional lipase−colipase−micelle ternary complex (*7*). Finally, the reduced activities of both F30HPL and F252HPL with respect to wtHPL further suggest that Trp residues at both positions 30 and 252 may also directly or indirectly contribute to an optimal catalytic activity.

Steady-State Fluorescence Spectroscopy of HPL Derivatives. The fluorescence spectrum of wtHPL (Figure 3) corresponds well to the previously reported spectrum (*18*). The rather red-shifted maximum emission wavelength (λ_{max} = 336 ± 1 nm) as well as the rather broad width at half-maximum (61 nm) indicated that the Trp residues were, on average, significantly exposed to the solvent (Table 1). This conclusion was somewhat unexpected from the calculated fractions of solvent exposure indicating that four Trp residues were fully buried (Trp86, Trp106, Trp252, and Trp402), two were moderately exposed to solvent (Trp17 and Trp338), and only one (Trp30) was largely exposed to solvent (see the legend of Figure 1). This suggests that the fluorescence of the solvent-exposed residue(s) dominates HPL fluorescence. Moreover, the HPL quantum yield (0.071 ± 0.003) was found to be only half of that of free Trp in water (*24*), suggesting that several Trp residues (especially the buried ones) may be only weakly fluorescent.

Table 2: Interchromophore Distances[a]

	Trp17	Trp30	Trp86	Trp106	Trp252	Trp338	Trp402
Trp17	–	15.9	25.7	16.2	18.3	42.5	64.9
Trp30	15.9	–	21.8	9.8	12.8	44.6	67.2
Trp86	25.7	21.8	–	12.5	14.2	23.9	48.4
Trp106	16.2	9.8	12.5	–	9.6	35.2	53.0
Trp252	18.3	12.8	14.2	9.6	–	34.6	54.8
Trp338	42.5	44.6	23.9	35.2	34.6	–	28.7
Trp402	64.9	67.2	48.4	53.0	54.8	28.7	–

[a] Trp−Trp distances were measured (in angstroms) between the CE3 atoms of the indole rings in the three-dimensional structure of van Tilbeurgh *et al*. (*19*).

From the substitution of a single Trp residue with Phe, two effects are expected on the quantum yield. The first obvious effect is associated with the loss of the contribution of the substituted residue to the overall HPL fluorescence. In this respect, if the individual quantum yield of the substituted residue is lower than that of wtHPL, the quantum yield of the single-point mutant is expected to be higher than the quantum yield of wtHPL. The second effect is linked to the loss of fluorescence resonance energy transfer (FRET) between the mutated Trp residue and the other Trp residues of the protein. According to the Förster theory, FRET is strongly dependent on the interchromophore distance and becomes negligible when this distance exceeds 2 times the Förster critical distance, R_0 (*26*). Since for Trp−Trp couples, R_0 is in the range of 4−16 Å, only couples separated by less than 32 Å should be considered (Table 2). In addition, since the upper limit of R_0 corresponds to the special case of Trp residues at low temperatures (*27*), the 32 Å limit is probably overestimated, and several examples in the literature (*28*, *29*) show that an upper limit of ~22 Å would be more reasonable for proteins in solution.

From the comparison of HPL mutants with wtHPL, the most striking changes are observed when Trp30 is mutated, yielding a quantum yield decrease of ~35%. If we assumed that the extinction coefficients of the various Trp residues are similar and FRET with Trp30 is negligible, a quantum yield of 0.22 could be calculated for this residue, suggesting that Trp30 contributes ~44% of the overall HPL fluorescence. Together with the dramatic change in quantum yield, substitution of Trp30 with Phe yields a dramatic 9 nm blue shift in λ_{max} and 11 nm decrease in $\Delta\lambda_{1/2}$ (Table 1), suggesting that the λ_{max} value of Trp30 may be strongly shifted to the red. Assuming that the maximum emission wavelength of wtHPL corresponds to the sum of the λ_{max} values of the individual Trp residues weighted by their quantum yield, we obtained for Trp30 a λ_{max} of ~348 nm, typical of a highly solvent exposed residue (*26*), in excellent agreement with the tertiary structure of HPL. Moreover, the λ_{max} value (327 nm) of the remaining Trp residues in F30HPL is typical of proteins with poorly solvent accessible Trp residues (*30*), again in line with HPL tertiary structure.

In contrast to the F30HPL mutant, all the other mutants (F17HPL, F86HPL, F252HPL, and F402HPL) exhibit large

Table 3: Time-Resolved Fluorescence and Acrylamide Quenching Parameters of HPL Derivatives at an Emission Wavelength of 340 nm

	τ_i [a] (ns)	α_i[a]	f_i[a]	$\langle\tau\rangle$[a] (ns)	k_{qi}[b] (M^{-1} s^{-1})	V_i[b] (M^{-1})
wtHPL	0.29 ± 0.01	0.54 ± 0.03	0.10 ± 0.01	1.56 ± 0.03		
	1.61 ± 0.05	0.33 ± 0.01	0.34 ± 0.02		1.0×10^9	0.5
	6.77 ± 0.02	0.13 ± 0.01	0.56 ± 0.01		1.5×10^9	0.8
F17HPL	0.34 ± 0.01	0.65 ± 0.01	0.15 ± 0.01	1.50 ± 0.02		
	1.65 ± 0.09	0.22 ± 0.01	0.24 ± 0.01		1.2×10^9	0.5
	7.08 ± 0.13	0.13 ± 0.01	0.61 ± 0.01		1.4×10^9	0.9
F30HPL	0.35 ± 0.01	0.62 ± 0.01	0.22 ± 0.01	1.00 ± 0.01		
	1.46 ± 0.12	0.29 ± 0.01	0.42 ± 0.05		2.1×10^9	0.5
	4.10 ± 0.20	0.09 ± 0.03	0.36 ± 0.05		2.7×10^8	0.1
F86HPL	0.31 ± 0.01	0.41 ± 0.03	0.07 ± 0.01	1.90 ± 0.06		
	1.54 ± 0.08	0.44 ± 0.03	0.35 ± 0.02			
	7.36 ± 0.05	0.15 ± 0.01	0.58 ± 0.02			
F252HPL	0.29 ± 0.01	0.38 ± 0.01	0.06 ± 0.01	1.89 ± 0.04		
	1.60 ± 0.01	0.49 ± 0.01	0.42 ± 0.02			
	7.67 ± 0.05	0.13 ± 0.01	0.53 ± 0.02			
F402HPL	0.30 ± 0.03	0.60 ± 0.01	0.11 ± 0.01	1.60 ± 0.05		
	1.60 ± 0.11	0.26 ± 0.02	0.26 ± 0.01			
	7.23 ± 0.03	0.14 ± 0.01	0.62 ± 0.01			

[a] The fluorescence lifetimes (τ_i), the relative amplitudes (α_i), the fractional intensities (f_i), and the mean lifetimes ($\langle\tau\rangle$) are expressed as means ± the standard error of the mean for three experiments. [b] The bimolecular quenching constant (k_{qi}) and the static quenching constant (V_i) were obtained by fitting the data in Figure 6 to eq 3. The errors on both parameters are ~10−20%.

(25−48%) increases in the fluorescence quantum yield. This suggests that in contrast to Trp30, neither Trp17, Trp86, Trp252, nor Trp402 is associated with a large quantum yield. If it is assumed that the extinction coefficients of the various Trp residues are similar and no Trp−Trp homotransfer occurs, the largest HPL quantum yield increase would be expected to result from the substitution of a nonfluorescent Trp residue, leading to a quantum yield of 0.083. Since the measured quantum yields are all larger than this value, this suggests that the initial assumptions are not valid. Since Trp402 is far (>28 Å) from all the other Trp residues, the loss of Trp−Trp homotransfer is expected to play only a very limited role, and thus, the slightly higher ϕ value of F402HPL as compared to the theoretical value of 0.083 may be ascribed to an extinction coefficient of Trp402 that is smaller than the average extinction coefficient of the remaining residues. Since the variations in extinction coefficients are usually limited, the higher quantum yields observed for the other mutants are thought to reflect losses in Trp−Trp homotransfer, with the mutated residues mainly acting as acceptors. In contrast, since the λ_{max} of these mutants was similar to or even higher than that of wtHPL, the relative contribution of Trp30 in the fluorescence of these mutants is expected to be similar or even greater than in wtHPL, suggesting that Trp30 may act mainly as a donor in Trp−Trp homotransfer. As a consequence, the 0.22 quantum yield and 44% contribution of Trp30 fluorescence to the overall wtHPL fluorescence calculated above may be considered lower limits, further suggesting that HPL fluorescence is dominated by the fluorescence properties of Trp30. In contrast, the residues at positions 17, 86, and 252 seem to be only weakly fluorescent but act as acceptors in Trp−Trp homotransfer.

Time-Resolved Fluorescence of HPL Derivatives. The fluorescence decay parameters of wtHPL and its mutants were determined by the single-photon counting time-correlated technique at emission wavelengths from 310 to 400 nm. A comparison between wtHPL and its various mutants was first based on the parameters determined at 340 nm, close to the maximum emission wavelength of wtHPL (Table 3). Three lifetimes were obtained for each derivative. The

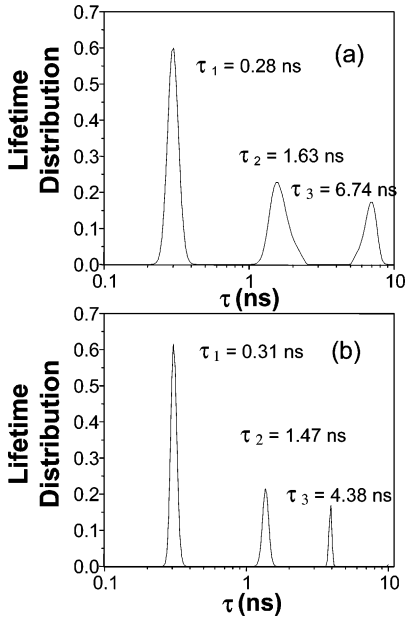

FIGURE 4: Fluorescence lifetime distributions of wtHPL and F30HPL. The lifetime distributions were recovered by MEM for (a) wtHPL and (b) F30HPL.

decay of wtHPL is dominated by the intermediate (1.61 ns) and the long-lived component (6.77 ns) that contribute to 34 and 56% of the total fluorescence intensity, respectively. In contrast, the short-lived component (0.29 ns) is by far the dominant species in amplitude (α_1 = 54%) (Figure 4).

The most remarkable change with respect to wtHPL was obtained with F30HPL, since the long-lived component, τ_3, decreases to 4.10 ns and its relative amplitude was decreased by approximately one-third compared with that of wtHPL. In contrast, the F30 mutation induces only a limited decrease in the intermediate lifetime as well as a slight increase in the amplitude associated with the short-lived lifetime. From these observations, one might speculate that the τ_3 value in wtHPL corresponds to a linear combination between a 4.10 ns component and a much longer component specifically associated with the Trp30 residue. The value of this latter component will depend of course on its relative amplitude

with respect to the 4.10 ns component. If we assume that the 4.10 ns component contributes with the same amplitude in wtHPL as in F30HPL, it follows that the lifetime associated with Trp30 would be as high as 13 ns. This conclusion is unlikely because lifetimes differing by a factor of 3.2 would be easily resolved (*31*, *32*). In addition, the 6.77 ns peak in wtHPL lifetime distributions is rather narrow (Figure 4) and thus could hardly correspond to an overlap of such widely separated components. A more reasonable explanation would be that deletion of Trp30 leads to the disappearance of FRET with another Trp residue, acting as a donor. This may in turn lead to an increase in the donor lifetime and explain the appearance of the 4.10 ns component in F30HPL. Alternatively, the substitution of Trp30 with a Phe residue may induce some local tertiary structure changes that release the quenching of the proximal Trp residues (at positions 106 and 252) and lead to the appearance of the 4.10 ns component in one of these residues. It thus results from our data that the 6.77 ns lifetime in wtHPL could be specifically associated with Trp30.

In contrast to F30HPL, all the other derivatives show a significant increase in τ_3 but no change in its amplitude. This increase in τ_3 may be tentatively ascribed to a loss of energy transfer between Trp30 and the substituted Trp residues. In line with this conclusion, the largest increase in τ_3 was observed when Trp252, one of the residues closest to Trp30 (Table 2), was substituted. The τ_1 and τ_2 values were not significantly affected by the mutations. In contrast, the changes in the amplitudes of these two lifetimes with respect to wtHPL allow us to distinguish two classes (Table 3). In the first class comprising the F17HPL and F402HPL derivatives, the amplitude associated with τ_2 decreases to the benefit of that associated with τ_1, whereas the reverse behavior was observed for F86HPL and F252HPL, which constitute the second class. It follows that Trp residues at positions 17 and 402 strongly contribute to the τ_2 value of wtHPL, while Trp residues at positions 86 and 252 contribute to the τ_1 value of wtHPL.

By multiplying the steady-state fluorescence intensity with the fractional intensities at the corresponding wavelengths, we obtained the decay-associated spectra (Figure 5). Noticeably, the three lifetimes of the various HPL derivatives were almost independent of the emission wavelength, indicating that relaxation of the Trp environment, at least for the most strongly emitting ones, is unlikely (*33*). The maximum emission wavelength of the spectrum associated with τ_3 was ~345 nm for all the derivatives with the exception of F30HPL. This maximum emission wavelength is close to that of Trp in water (350 nm), confirming that the component contributing most heavily to τ_3 is largely solvent-exposed and could thus be attributed to the Trp30 residue. In contrast, the maximum emission wavelength of the spectrum associated with τ_3 in F30HPL was shifted to the blue (330 nm), suggesting that τ_3 may be associated with a buried or poorly solvent exposed residue(s) in this mutant. A similar conclusion applies for the Trp residues associated with the τ_1 and τ_2 lifetimes in all HPL derivatives since the maximum emission wavelengths of their associated spectra were approximately 320−330 nm.

Moreover, the ratio of the area of each DAS to that of the steady-state fluorescence spectrum allowed us to determine the wavelength-independent fractional intensity (f_i^c) associated with each lifetime. This in turn allowed us to determine the wavelength-independent amplitude fraction (α_i^c) by solving the system of three equations:

$$f_i^c = \alpha_i^c \tau_i / \sum_{j=1}^{3} \alpha_j^c \tau_j \qquad (2)$$

where $i = 1-3$. The values reported in Table 4 indicate that the true contributions of τ_1 to τ_3 in the various HPL derivatives are similar to those deduced at 340 nm. From the α_i^c values, it was then possible to deduce the wavelength-independent mean lifetime from the relationship $\langle\tau\rangle^c = \sum_i \alpha_i^c \tau_i$, and finally, the average radiative rate constant, k_r, from the relationship $k_r = Q/\langle\tau\rangle^c$ (*34*). The k_r value of

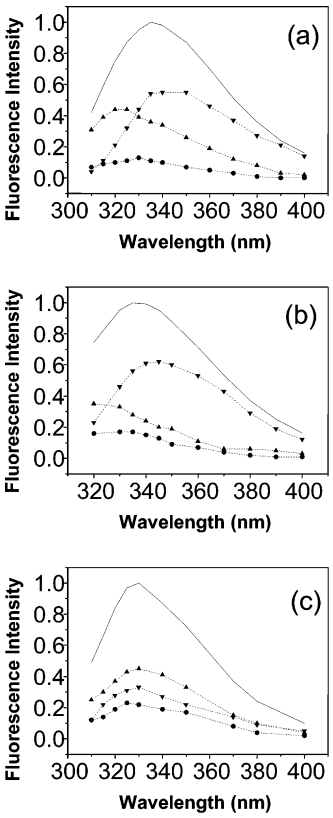

FIGURE 5: Decay-associated spectra of (a) wtHPL, (b) F252HPL, and (c) F30HPL. For each derivative, the steady-state fluorescence spectrum (—) was resolved into three spectra associated with τ_1 (●), τ_2 (▲), and τ_3 (▼).

Table 4: Wavelength-Independent Time-Resolved Fluorescence Parameters[a]

	τ_i^c (ns)	α_i^c	f_i^c	$\langle\tau\rangle^c$ (ns)	k_r (ns^{-1})
wtHPL	0.28 ± 0.03	0.52	0.09	1.59	0.033
	1.63 ± 0.21	0.35	0.36		
	6.74 ± 0.13	0.13	0.55		
F17HPL	0.35 ± 0.02	0.60	0.12	1.76	0.046
	1.78 ± 0.14	0.24	0.24		
	7.02 ± 0.12	0.16	0.64		
F30HPL	0.34 ± 0.04	0.63	0.22	0.95	0.046
	1.44 ± 0.10	0.29	0.43		
	4.00 ± 0.20	0.08	0.35		

[a] The wavelength-independent time-resolved fluorescence parameters were calculated as described in the text. The lifetimes (τ_i^c) correspond to the mean ± the standard deviation of the lifetimes determined at emission wavelengths ranging from 310 to 400 nm. The standard deviations for α_i^c and f_i^c are ~10% of their values.

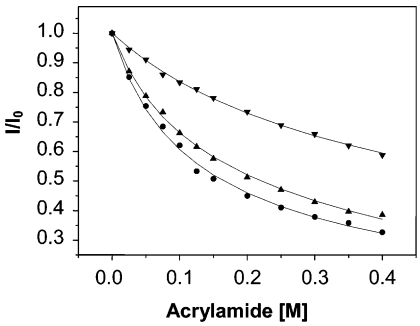

FIGURE 6: Quenching of HPL derivatives with acrylamide. The concentrations of wtHPL (▲), F17HPL (●), and F30HPL (▼) were 2 μM in the same buffer as in Figure 2. Excitation and emission wavelengths were 295 and 340 nm, respectively. Solid lines correspond to the fits of the experimental points to eq 3 and the parameters in Table 3.

F17HPL was similar to the value of 0.046 ns^{-1} for *N*-acetyltryptophanamide in water (*26*, *35*), in line with the predominant contribution of the solvent-exposed Trp30 residue to the steady-state fluorescence of this mutant. The significantly lower value obtained with wtHPL could not be correlated to any obvious change in the maximum emission wavelength (and thus in the environment of the Trp residues) but may probably be linked to static quenching.

Fluorescence Quenching by Acrylamide. Quenching experiments were performed with the external uncharged acrylamide quencher that can penetrate a protein matrix and quench both solvent-exposed and buried Trp residues. Because of the multicomponent decay of HPL derivatives, the inhibition curves recorded at the maximum emission wavelength (Figure 6) were fitted with a modified Stern−Volmer equation:

$$\frac{I}{I_0} = \sum_i \frac{f_i}{(1 + k_{qi}\tau_i[Q])\exp(V_i[Q])} \qquad (3)$$

where k_{qi} is the bimolecular quenching constant for the residues associated with the τ_i lifetime, V_i is the static quenching constant, and [Q] is the concentration of the quencher. In line with the significant exposure of Trp30 to solvent, rather high k_q and V values were associated with the τ_3 lifetime of both wtHPL and F17HPL (Table 3). In sharp contrast, the low k_{q3} and V_3 parameters for F30HPL clearly indicate that the residues mainly contributing to the τ_3 lifetime in F30HPL are embedded ones, in excellent agreement with the blue-shifted maximum emission wavelength of its DAS (Figure 5). Finally, the rather high k_{q2} and V_2 values associated with F30HPL, and to a lesser extent with wtHPL and F17HPL, suggest that the Trp residues mainly contributing to the τ_2 lifetime of these three mutants are at least partly solvent-exposed.

DISCUSSION

In the study presented here, the steady-state and time-resolved fluorescence parameters of wtHPL were investigated and compared to those of single-point mutants in which one of the seven Trp residues of HPL has been substituted with a Phe residue. One of the most striking features is that substitution of Trp30 induces a dramatic quantum yield decrease correlated with a dramatic decrease in the long-lived lifetime value, a large blue shift in λ_{max}, and a large decrease in accessibility to acrylamide. These data suggest that the fluorescence of wtHPL is dominated by the fluorescence of the solvent-exposed Trp30 residue that contributes at least to 44% of the overall wtHPL fluorescence. Moreover, this residue is characterized by a 6.77 ns lifetime that is consistent with its large estimated quantum yield ($\phi > 0.22$). Both the large lifetime and quantum yield values associated with the Trp30 residue are not unprecedented for solvent-exposed Trp residues since similar values have been reported for the Trp37 residue in the distal finger motif of the nucleocapsid protein from HIV (*36*, *37*). This 6.77 ns lifetime constitutes a specific signature of Trp30 in wtHPL and enables a selective monitoring of the local changes in the Trp30 environment despite the presence of seven Trp residues in wtHPL.

Comparison of wtHPL with its mutants further suggests that the lifetime associated with the Trp30 residue is sensitive to FRET with other Trp residues on the same protein. This is especially true for the proximal Trp residues at positions 17, 86, and 252 (Table 2) since substitution of either of these residues leads to a significant increase in τ_3 and quantum yield (Table 3). Additionally, the couples between Trp30 and each of these residues are likely characterized by a rather high Förster critical distance (R_0) that further contributes to efficient FRET. Indeed, the R_0 value mainly depends on the spectral overlap between the emission spectrum of the donor and the absorption spectrum of the acceptor, the quantum yield of the donor, and the orientation between the chromophores. Since (i) Trp30 has a high quantum yield, (ii) the spectral overlap is optimal when a Trp residue in a polar environment transfers its energy to a Trp residue in a nonpolar environment, and (iii) the rotational freedom of solvent-exposed Trp residues prevents to some extent adverse orientations, a high R_0 value and, thus, an efficient FRET are believed to occur between Trp30, acting as a donor, and any of the proximal buried or partially solvent-exposed Trp residues.

In contrast to τ_3, the two remaining lifetimes could not be specifically attributed to a single Trp residue. Since the decay of individual Trp residues generally involves two or three lifetimes and since the lifetime measurements and analysis do not allow discrimination of components that differ by a factor of less than 1.4−1.7 (*31*, *32*), the τ_1 and τ_2 lifetimes of HPL are expected to be complicated functions of the lifetimes of the various Trp residues. Nevertheless, from the comparison of the single-point mutants with wtHPL, it could be concluded that Trp17 and Trp402 strongly contribute to the τ_2 lifetime of wtHPL while Trp86 and Trp252 mainly contribute to τ_1. The contribution of the significantly solvent-exposed Trp17 residue in the τ_2 lifetime is further substantiated by the rather large bimolecular quenching constant associated with this lifetime in wtHPL and F30HPL (Table 3). However, since a large bimolecular quenching constant is also observed for the τ_2 lifetime of F17HPL, it is further suggested that the second partially solvent exposed Trp residue (at position 338) may also contribute to the τ_2 lifetime. Since an even larger bimolecular quenching constant is observed for the τ_2 lifetime of F30HPL, one may speculate that some local structural changes even increase the accessibility of Trp17 and/or Trp338 residues in this mutant. Finally, from the low accessibility of the F30HPL τ_3 lifetime

Table 5: Distances between Trp and the Closest Quenching Groups in wtHPL[a]

	histidine (Å)	Cys−Cys (Å)	cysteine (Å)
Trp86	6.61 (75) 5.01 (151) 8.87 (263)	8.98−9.16 (90−101)	8.12 (103)
Trp106	2.92 (75)	−	−
Trp252	7.33 (75) 5.60 (263)	−	9.37 (181)
Trp17, -30, -338, and -402	−	−	−

[a] The distances of closest approach between the various Trp residues and their neighboring quenching groups were calculated from the three-dimensional structure of HPL (*19*). Only quenchers closer than 10 Å were mentioned. The positions of the quenching amino acids are given in parentheses.

to acrylamide, one may speculate that this lifetime is associated with one of the two embedded Trp residues (at positions 106 and 252) close to Trp30.

In proteins, the major quenchers of Trp fluorescence are the side chains of histidine (in its protonated form) (*38*), cysteine and its disulfide bridge (*39*), and the peptide backbone (*40*). As a consequence, the distances between the various Trp residues and their neighboring His, Cys, and cystine groups were measured in the crystal structure (Table 5). In keeping with our data, Trp86 was found to be close to the lateral chains of His151, His75, and Cys103 as well as to the disulfide bridge between Cys90 and Cys101 and is thus expected to be strongly quenched. Likewise, the contact between Trp106 and His75 suggests that this Trp residue may be strongly quenched, at least at pH values where the His residue is protonated. In contrast, the less quenched fluorescence inferred for the Trp residues at positions 17, 30, 338, and 402 could be partly related to the absence of proximal His, Cys, or disulfide bridges in their environment. In fact, it is likely that charge transfer from the excited indole moiety to the carbonyl group of the peptide backbone is probably the main nonradiative pathway in these Trp residues (*41*). However, measurement of the distances between the CE3 atom of their indole ring and the neighboring carbonyl groups shows no obvious correlation with their deduced fluorescence properties (data not shown). This may be due to the fact that quenching is highly dynamic and depends on both the distance and orientation of the quencher as well as on the collisional frequency (*42*). Moreover, Trp residues are usually present under various rotameric forms (*43*) that differ in their χ_1 and χ_2 angles and, thus, by the distances between the indole moiety and the quenchers. Since the preferred conformers in solution are not necessarily the same as those in crystals (*42*), there may be for Trp30 another rotameric form that further removes the lateral chain from its neighboring quenchers.

In conclusion, the time-resolved fluorescence parameters of HPL enable us to selectively and sensitively monitor Trp30 environmental changes, despite the presence of seven Trp residues in wtHPL. Some additional but more limited information about the other Trp residues (mainly Trp17, Trp338, and Trp402) that also significantly contributes to HPL fluorescence could also be gained. Additional work to monitor by this tool the conformational changes accompanying the transition between the inactive and active forms of HPL is actually in progress. The specific signature of Trp30 will also be a useful tool for further investigating the positioning of lipase at the water−lipid interface.

REFERENCES

1. Sarda, L., and Desnuelle, P. (1958) *Biochim. Biophys. Acta 30*, 513−521.
2. Borgstrom, B. (1975) *J. Lipid Res. 16*, 411−417.
3. Chapus, C., Sari, H., Semeriva, M., and Desnuelle, P. (1975) *FEBS Lett. 58*, 155−158.
4. Vandermeers, A., Vandermeers-Piret, M. C., Rathe, J., and Christophe, J. (1975) *FEBS Lett. 49*, 334−337.
5. Winkler, F. K., D'Arcy, A., and Hunziker, W. (1990) *Nature 343*, 771−774.
6. van Tilbeurgh, H., Egloff, M. P., Martinez, C., Rugani, N., Verger, R., and Cambillau, C. (1993) *Nature 362*, 814−820.
7. Hermoso, J., Pignol, D., Penel, S., Roth, M., Chapus, C., and Fontecilla-Camps, J. C. (1997) *EMBO J. 16*, 5531−5536.
8. Ayvazian, L., Crenon, I., Hermoso, J., Pignol, D., Chapus, C., and Kerfelec, B. (1998) *J. Biol. Chem. 273*, 33604−33609.
9. Osterlund, T., Beussman, D. J., Julenius, K., Poon, P. H., Linse, S., Shabanowitz, J., Hunt, D. F., Schotz, M. C., Derewenda, Z. S., and Holm, C. (1999) *J. Biol. Chem. 274*, 15382−15388.
10. Jutila, A., Zhu, K., Patkar, S. A., Vind, J., Svendsen, A., and Kinnunen, P. K. (2000) *Biophys. J. 78*, 1634−1642.
11. Cajal, Y., Svendsen, A., De Bolos, J., Patkar, S. A., and Alsina, M. A. (2000) *Biochimie 82*, 1053−1061.
12. Cajal, Y., Svendsen, A., Girona, V., Patkar, S. A., and Alsina, M. A. (2000) *Biochemistry 39*, 413−423.
13. Graupner, M., Haalck, L., Spener, F., Lindner, H., Glatter, O., Paltauf, F., and Hermetter, A. (1999) *Biophys. J. 77*, 493−504.
14. Zhu, K., Jutila, A., Tuominen, E. K., Patkar, S. A., Svendsen, A., and Kinnunen, P. K. (2001) *Biochim. Biophys. Acta 1547*, 329−338.
15. Zhu, K., Jutila, A., Tuominen, E. K., and Kinnunen, P. K. (2001) *Protein Sci. 10*, 339−351.
16. Zhu, K., Jutila, A., and Kinnunen, P. K. (2000) *Protein Sci. 9*, 598−609.
17. Melo, E. P., Taipa, M. A., Castellar, M. R., Costa, S. M., and Cabral, J. M. (2000) *Biophys. Chem. 87*, 111−120.
18. Luthi-Peng, Q., and Winkler, F. K. (1992) *Eur. J. Biochem. 205*, 383−390.
19. van Tilbeurgh, H., Sarda, L., Verger, R., and Cambillau, C. (1992) *Nature 359*, 159−162.
20. Sanger, F., Nicklen, S., and Coulson, A. R. (1977) *Proc. Natl. Acad. Sci. U.S.A. 74*, 5463−5467.
21. Ayvazian, L., Crenon, I., Granon, S., Chapus, C., and Kerfelec, B. (1996) *Protein Eng. 9*, 707−711.
22. Laemmli, U. K. (1970) *Nature 227*, 680−685.
23. Burnette, W. N. (1981) *Anal. Biochem. 112*, 195−203.
24. Eisinger, J., and Navon, G. (1969) *J. Chem. Phys. 50*, 2069−2077.
25. Hermoso, J., Pignol, D., Kerfelec, B., Crenon, I., Chapus, C., and Fontecilla-Camps, J. C. (1996) *J. Biol. Chem. 271*, 18007−18016.
26. Lakowicz, J. R. (1999) *Principles of Fluorescence Spectroscopy*, 2nd ed., Plenum Press, New York.
27. Weber, G. (1960) *Biochem. J. 75*, 335−345.
28. Willaert, K., Loewenthal, R., Sancho, J., Froeyen, M., Fersht, A., and Engelborghs, Y. (1992) *Biochemistry 31*, 711−716.
29. Bombarda, E., Ababou, A., Vuilleumier, C., Gérard, D., Roques, B. P., Piemont, E., and Mély, Y. (1999) *Biophys. J. 76*, 1561−1570.
30. Eftink, M. R. (1991) in *Topics in Fluorescence Spectroscopy* (Lakowicz, J. R., Ed.) pp 53−126, Plenum Press, New York.
31. Siemiarczuk, A., Wagner, B. D., and Ware, W. R. (1990) *J. Phys. Chem. 94*, 1661−1666.
32. Vix, A., and Lami, H. (1995) *Biophys. J. 68*, 1145−1151.
33. Demchenko, A. P. (1992) in *Topics in Fluorescence Spectroscopy* (Lakowicz, J. R., Ed.) pp 65−111, Plenum Press, New York.
34. Sillen, A., and Engelborghs, Y. (1998) *Photochem. Photobiol. 67*, 475−486.
35. Werner, T. C., and Förster, L. C. (1979) *Photochem. Photobiol. 29*, 905−914.
36. Mély, Y., de Rocquigny, H., Piemont, E., Demene, H., Jullian, N., Fournie-Zaluski, M. C., Roques, B., and Gérard, D. (1993) *Biochim. Biophys. Acta 1161*, 6−18.

37. Mély, Y., De Rocquigny, H., Morellet, N., Roques, B. P., and Gérard, D. (1996) *Biochemistry 35*, 5175−5182.
38. Shinitzky, M., and Goldman, R. (1967) *Eur. J. Biochem. 3*, 139−144.
39. Cowgill, R. W. (1967) *Biochim. Biophys. Acta 140*, 552−554.
40. Chen, R. F., Knutson, J. R., Ziffer, H., and Porter, D. (1991) *Biochemistry 30*, 5184−5195.
41. Chen, Y., Liu, B., Yu, H., and Barkley, M. D. (1996) *J. Am. Chem. Soc. 118*, 9271−9278.
42. Sillen, A., Hennecke, J., Roethlisberger, D., Glockshuber, R., and Engelborghs, Y. (1999) *Proteins 37*, 253−263.
43. Szabo, A. G., and Rayner, D. M. (1980) *Biochem. Biophys. Res. Commun. 94*, 909−915.

BI034900E